

Published in final edited form as:

*Cell*. 2013 August 15; 154(4): 763–774. doi:10.1016/j.cell.2013.07.015.

## Structural basis for ebolavirus matrix assembly and budding; protein plasticity allows multiple functions

Zachary A. Bornholdt<sup>1</sup>, Takeshi Noda<sup>2</sup>, Dafna M. Abelson<sup>1</sup>, Peter Halfmann<sup>3</sup>, Malcolm Wood<sup>4</sup>, Yoshihiro Kawaoka<sup>2,3,5</sup>, and Erica Ollmann Saphire<sup>1,6</sup>

<sup>1</sup>Dept. of Immunology and Microbial Science, The Scripps Research Institute, La Jolla, California

<sup>2</sup>International Research Center for Infectious Diseases, Institute of Medical Science, University of Tokyo, Tokyo, Japan

<sup>3</sup>Department of Pathobiological Sciences, School of Veterinary Medicine, University of Wisconsin, Madison, Wisconsin

<sup>4</sup>Core Microscopy Service, The Scripps Research Institute, La Jolla, California

<sup>5</sup>Division of Virology, Department of Microbiology and Immunology, Institute of Medical Science, University of Tokyo, Tokyo, Japan

<sup>6</sup>The Skaggs Institute for Chemical Biology, The Scripps Research Institute, La Jolla, California

### Summary

Proteins, particularly viral proteins, can be multifunctional, but the mechanism(s) behind this trait are not fully understood. Here, we illustrate through multiple crystal structures, biochemistry and cellular microscopy that VP40 rearranges into different structures, each with a distinct function required for the ebolavirus life cycle. A butterfly-shaped VP40 dimer trafficks to the cellular membrane. There, electrostatic interactions trigger rearrangement of the polypeptide into a linear hexamer. These hexamers construct a multi-layered, filamentous matrix structure that is critical for budding and resembles tomograms of authentic virions. A third structure of VP40, formed by a different rearrangement, is not involved in virus assembly, but instead uniquely binds RNA to regulate viral transcription inside infected cells. These results provide a functional model for ebolavirus matrix assembly and the other roles of VP40 in the virus life cycle, and demonstrate how a single, wild-type, unmodified polypeptide can assemble into different structures for different functions.

### Introduction

Ebolaviruses cause severe hemorrhagic fever with up to 90% lethality and are considered potential biological weapons (Bwaka et al., 1999; Kuhn, 2008). There are five antigenically

© 2013 Elsevier Inc. All rights reserved.

**Publisher's Disclaimer:** This is a PDF file of an unedited manuscript that has been accepted for publication. As a service to our customers we are providing this early version of the manuscript. The manuscript will undergo copyediting, typesetting, and review of the resulting proof before it is published in its final citable form. Please note that during the production process errors may be discovered which could affect the content, and all legal disclaimers that apply to the journal pertain.

distinct ebolaviruses, each named after the location of the outbreak in which they were first discovered. Of these, the two most common are Ebola virus and Sudan virus (Kuhn et al., 2013). Ebolaviruses encode just seven genes, and are distinguished by their pleomorphic filamentous morphology (Kuhn, 2008). Ebolaviruses assemble and bud from the cell membrane in a process driven by the viral matrix protein VP40 (Harty et al., 2000; Panchal et al., 2003). VP40 alone is sufficient to assemble and bud filamentous virus-like particles (VLPs) from cells (Geisbert and Jahrling, 1995; Johnson et al., 2006; Noda et al., 2002).

The first crystal structure of VP40 suggested that this protein is monomeric (Dessen et al., 2000a; Dessen et al., 2000b). The structure revealed that VP40 contains distinct N- and C-terminal domains (NTD and CTD respectively), both essential for trafficking to and interaction with the membrane (Harty, 2009; Jasenosky et al., 2001). The limited number of contacts observed between the NTD and CTD suggested that they are tenuously connected and could separate to assemble a different structure (Dessen et al., 2000b; Gomis-Ruth et al., 2003). Indeed, when VP40 is incubated with urea and RNA or liposomes, conformational changes occur and the NTD then drives the assembly of RNA-binding ring structures (Harty, 2009). A crystal structure of a VP40 ring was solved by expressing the VP40 NTD alone. In the structure, eight VP40 NTDs assemble into a ring with each NTD bound to an RNA trinucleotide (Gomis-Ruth et al., 2003).

Currently, the VP40 ring and the interfaces by which it assembles provide the only known structural model of how VP40 might assemble the ebolavirus matrix. However, these rings are observed only in infected cells, not in mature purified ebolaviruses (Gomis-Ruth et al., 2003), suggesting the ring structure is not involved in matrix assembly. Instead, the RNA-binding VP40 rings likely play a critical, but currently undefined role inside the infected cell (Gomis-Ruth et al., 2003; Hoenen et al., 2010a).

Despite the wealth of structural and biochemical data, no cohesive model exists for how the ebolavirus matrix is assembled. It is currently unclear what structure of VP40 migrates to the cell membrane and how that structure is triggered to further oligomerize into the viral matrix. Although RNA binding by VP40 is critical to the viral life cycle (Hoenen et al., 2005), the exact role of the VP40 RNA-binding ring has remained elusive. In addition and perhaps most significantly, the structural arrangement of VP40 within the ebolavirus matrix remains unknown. Here we set out to provide a structurally and biologically supported model of VP40-driven matrix assembly and elucidate the different roles VP40 plays in the ebolavirus life cycle.

We first purified VP40 and determined that it is a dimer in solution, not a monomer as previously thought (Dessen et al., 2000b). We then determined multiple crystal structures of dimeric VP40, from Ebola virus and Sudan virus, revealing a conserved dimeric interface. Targeted mutagenesis of the dimer interface abolishes trafficking of VP40 to the cell membrane and budding of VLPs, suggesting that the VP40 dimer is a critical precursor of the viral matrix. We next analyzed a conserved CTD-to-CTD interface by which VP40 dimers are linked together in crystals. Structure-based mutagenesis of the CTD-to-CTD interface abolishes assembly and budding of virus-like particles, but not trafficking to or

interactions with the membrane. Thus, assembly of VP40 dimers via CTD interactions likely represents a critical step in matrix assembly.

We next turned our attention to understanding how the VP40 dimer interacts with the membrane and conformational changes believed to occur at the membrane important to matrix assembly. Previous work has demonstrated that electrostatic interactions between the VP40 CTD and the membrane are likely important to matrix assembly (Adu-Gyamfi et al., 2012; Ruigrok et al., 2000; Scianimanico et al., 2000). Through targeted mutagenesis, we identified a conserved basic patch in the CTD that mediates both membrane interaction and subsequent matrix assembly events. An electrostatic mimic of the membrane was found to trigger conformational rearrangement of VP40 dimers into a novel, linear hexameric assembly. In the crystal structure of this assembly, VP40 hexamers also connect into continuous filaments via the conserved CTD interactions. We propose that the VP40 hexamer structure represents a building block of the flexible, filamentous ebolavirus matrix. Our hexameric VP40 structure suggests VP40 assembles into a multilayered matrix along the membrane, which is consistent with recent electron tomographic analysis of filoviruses in scale, dimension and layered construction (Beniac et al., 2012; Bharat et al., 2011).

We also determined that the VP40 RNA-binding ring structure, while derived from the VP40 dimer, is not involved in or required for matrix assembly and budding. Instead, we show that the VP40 ring plays a distinct and critical role in regulation of viral transcription inside infected cells, and that this function is dependent on its unique RNA-binding capability.

Taken together, our results illustrate that the highly plastic VP40 polypeptide is able to rearrange itself into distinct structural assemblies. Each of these distinct structures is assembled by the unmodified wild-type polypeptide and each structure is required for a separate and essential function in the virus life cycle: a dimeric precursor critical for cellular trafficking, a hexameric structural component for the viral matrix assembly, and a nonstructural RNA-binding ring structure essential for regulating viral transcription. Thus, the physical plasticity inherent in VP40 demonstrates how a protein structure can expand the functional repertoire of a single viral gene.

## Results

### Ebolavirus VP40 is a dimer in solution

Three constructs of VP40 were expressed without fusion partners, purified, and subjected to size exclusion chromatography and multi-angle light scattering (SEC-MALS). These included wild-type full-length Ebola virus VP40 (WT-VP40E) and Ebola and Sudan virus VP40 with a deletion of 43 residues from the disordered N-terminus in order to improve crystal diffraction (VP40S<sub>N</sub> and VP40E<sub>N</sub>, respectively) (Figure 1A). All three VP40 proteins consistently elute from size exclusion columns as dimers and maintain molecular weights consistent with a dimer via SEC-MALS analysis, a more sensitive method for accurate molecular weight determination than size exclusion chromatography alone (Wyatt, 1998) (Figure S1). This result is in contrast to previous work in which VP40 (also

containing an N-terminal deletion of 30 residues) was characterized as a monomer (VP40E<sub>M</sub>) (Dessen et al., 2000a; Dessen et al., 2000b).

### Crystal structures of Sudan and Ebola virus VP40 identify the dimeric interface of ebolavirus VP40

The VP40S<sub>N</sub> protein crystallizes in the space group C2 with one protomer in the crystallographic asymmetric unit (ASU) and diffracts to 1.8 Å resolution. The VP40E<sub>N</sub> protein crystallizes in the space group P6<sub>2</sub> with four protomers in the ASU and diffracts to 3.1 Å resolution. In all these crystal structures, the overall protein architecture remains conserved with the previously determined VP40E<sub>M</sub> (Dessen et al., 2000b): the NTD contains a β-sandwich decorated by four small α-helices, while the CTD contains some disordered loop structure that links two small β-sheets and two α-helices. We detail here the structure of the dimeric interface conserved in the crystal structures (Figure 1).

There is one protein-protein interface that is completely conserved throughout crystals of VP40E<sub>N</sub> and VP40S<sub>N</sub>, suggesting that it assembles the in-solution dimer. The interface is between the NTDs of two VP40 protomers and buries 1500-1700 Å<sup>2</sup> of molecular surface, depending on the viral species (Figures 1B). Although not previously described, this dimeric interface is also conserved between symmetry-related protomers in the crystal packing of VP40E<sub>M</sub> (Dessen et al., 2000b). Overall, the dimers are structurally conserved with an r.m.s.d of 0.45 to 0.88 Å (Figure S2).

The VP40 dimeric interface involves residues 52-65 and 108-117, which encompass two α-helices (residues 61-65, and 108-116). Interactions within the VP40 dimeric interface have limited hydrogen bonding and are primarily hydrophobic in nature. The hydrophobic network in the dimer interface involves residues A55, H61, F108, T112, A113, M116 and L117, of which L117 appears to be of central importance. L117 extends into a hydrophobic pocket formed by residues H61, A55, M116 and F108 in the opposing subunit and appears to lock the VP40 protomers together into a dimer (Figure 1C).

### The dimer interface is essential for matrix assembly and viral budding

Mutagenesis was performed to verify the biological relevance of the conserved VP40 dimeric interface. Two mutations were made: L117R and T112R (VP40E<sub>N</sub>-L117R and VP40E<sub>N</sub>-T112R), as modeling suggested that the larger arginine side chain in these positions would disrupt the VP40 dimeric interface (Figure 2A). Indeed, purified VP40E<sub>N</sub>-L117R and VP40E<sub>N</sub>-T112R are primarily monomeric, but also assemble some RNA-binding ring structures (Figure S1). Thus the L117R and T112R mutations have not disrupted the tertiary structure of the VP40 NTD, as a properly-folded NTD is essential for ring assembly (Gomis-Ruth et al., 2003).

Western blot analysis of cells transfected with WT-VP40E or the mutants VP40E-L117R or VP40E-T112R showed that while WT-VP40E is successfully released from cells, both mutants are retained within the cell (Figure 2B). Indeed, immunofluorescence analysis (IFA) illustrated that WT-VP40E efficiently buds virus-like particles (VLPs), while both VP40E-L117R and VP40E-T112R mutants fail to migrate to the membrane or bud VLPs (Figure 2C). The IFA also indicated that VP40E-T112R has a propensity to form perinuclear

inclusions reminiscent of previously observed globular structures formed by VP40 oligomeric rings (Panchal et al., 2003). Transmission electron microscopy (TEM) further showed that while WT-VP40 assembles into filamentous VLPs and buds from the cell membrane, both VP40E-L117R and VP40E-T112R fail to bud and display no signs of assembly at the cell surface (Figure 2D). Thus, the L117R and T112R point mutations disrupt VP40 dimer formation, cellular trafficking, matrix assembly and budding of ebolavirus-like particles, but do not appear to impede the formation of VP40 ring oligomers (Figures 2D, S1).

### **VP40 dimers further assemble end-to-end into filaments which are essential for matrix assembly and budding**

In all crystal structures of VP40 containing its C-terminal domain, the VP40 dimers further assemble end-to-end into filaments through homologous interactions between their C-terminal domains (Figure 3A, S3). This primarily hydrophobic CTD-to-CTD interface involves residues L203, I237, M241, M305 and I307, and has a smooth topology along the buried surface. The lack of interdigitation along this hydrophobic interface potentially allows for torsional motion between the CTDs. Indeed, potential motion about this interface can be observed in the P<sub>6</sub><sub>2</sub> crystal packing of VP40E N, in which every other dimer is rotated by ~90° along this CTD-to-CTD interface (Figure S3).

Mutagenesis was performed to determine if the CTD-to-CTD interface was relevant to ebolavirus matrix assembly and formation of filamentous VLPs. Residue M241 is buried in the CTD-to-CTD interface but is not integral to the fold of the CTD. Modeling suggested that replacement of M241 with arginine would impair formation of the CTD-to-CTD interface, but would not disrupt VP40 dimerization (Figure 3A). Indeed, purified VP40E N-M241R remains primarily dimeric in solution (Figure S1), yet transfected VP40E-M241R does not assemble or bud filamentous VLPs (Figure 3B). The neighboring residue T242, unlike M241, is solvent exposed and does not contribute to the CTD-to-CTD interface. Hence, a control mutant, VP40E-T242R, was also generated to ensure that merely placing an arginine residue in this region of the CTD does not inhibit the function of VP40. As anticipated, VP40E-T242R successfully assembles and buds VLPs at wild-type levels (Figure 3B).

Interestingly, cells transfected with VP40E-M241R exhibit an exaggerated membrane ruffling morphology, indicating that VP40E-M241R migrates to and interacts with the cell membrane, but still fails to properly assemble the matrix and bud VLPs. This suggests that VP40E-M241R may assemble some intermediate or defective matrix structure along the membrane (Figure 3C, 3D). In order to determine how VP40E-M241R might be assembling, we determined a crystal structure of the mutant. Crystals of VP40E N-M241R belong to the space group P<sub>4</sub><sub>1</sub>2<sub>1</sub>2 and diffract to 4.15 Å. The VP40E N-M241R structure indicates the VP40 dimer is intact, but interactions along the CTD-to-CTD interface are limited by the M241R mutation. Within the crystal packing, VP40E N-M241R fails to assemble any filaments and only interacts with one neighboring dimer via a minimal and twisted CTD-to-CTD interface, with L203 and I307 at the center rather than M241 (Figure S3). This may explain why VP40E-M241R ruffles the cell membrane but fails to bud VLPs, as the M241R

mutation would allow for a limited assembly of dimers, initiating membrane curvature, but fails to complete assembly of the matrix to bud VLPs.

### **A second point mutation in the VP40 CTD-to-CTD interface automatically triggers oligomeric ring formation and RNA binding**

Residue I307, similar to M241, is also buried in the CTD-to-CTD interface and was mutated to arginine in order to further investigate the physiological relevance of that interface (Figure 3A). Curiously, the purified VP40E N-I307R mutant displays a unique phenotype, in that it does not yield the expected dimers, but instead exclusively forms RNA binding oligomeric rings ( $A_{260/280} > 1.0$ ) (Figures S4, S1).

Western blots of cells transfected with VP40E-I307R indicated that this mutation blocks assembly and budding of VLPs into the supernatant (Figure 3B). Further, IFA showed that in these cells VP40E-I307R does not migrate to the cellular membrane, but instead assembles into large globular structures around the nucleus (Figure 3C). These perinuclear assemblies are similar to those formed by VP40E-T112R (Figure 2C) and other ring-forming VP40 mutants (Panchal et al., 2003). A control mutant analogous to VP40E-T242R was also generated: VP40E-Q309R. Residue Q309 is in close proximity to I307 but is solvent exposed like T242, rather than buried in the CTD-to-CTD interface. As expected, cells transfected with VP40E-Q309R assemble and bud ebolavirus VLPs at wild-type levels (Figure 3B).

A different VP40 mutation, R134A, has been previously shown to eliminate binding of RNA, disrupt formation of VP40 rings, and yield wild-type VLP morphologies and levels of budding (Hoenen et al., 2005). Here we show that purified VP40E N-R134A remains a dimer and confirm that VP40E-R134A assembles and buds VLPs at wild-type levels (Figures 3, S1). We next generated a double mutant, VP40E-R134A/I307R, in which the I307R component would prevent CTD-mediated filament assembly and the R134A component would prevent I307R-induced RNA binding and ring formation. As anticipated, purified VP40E N-R134A/I307R mutant is a nucleic acid-free dimer in solution ( $A_{260/280} < 0.6$ ) (Figure S1). When transfected, VP40E-R134/I307R no longer forms perinuclear inclusions. Instead, it migrates to the cellular membrane, consistent with a dimeric VP40 phenotype (Figure 3C). Although VP40E-R134A/I307R is a membrane-trafficking dimer, it does not assemble or bud VLPs (Figure 3), consistent with disruption of the CTD-to-CTD interface by I307R. However, unlike VP40E-M241R, cells transfected with VP40E-R134A/I307R are devoid of membrane ruffles (Figure 3D). Modeling suggests that unlike M241R, the VP40E-I307R point mutation would strictly prohibit any CTD-to-CTD interactions. Thus, the lack of membrane ruffling is likely due to the inability of dimeric VP40E-R134A/I307R to further assemble via the CTD along the membrane.

Taken together, these results indicate that targeted mutations to the CTD-to-CTD interface (M241R and I307R) block matrix assembly and budding, while similar control mutations to nearby residues in the CTD not directly involved in the CTD-to-CTD interface (T242R and Q309R) have no effect on matrix assembly and budding. Thus, the CTD-to-CTD interface, by which VP40 dimers further assemble into filaments, appears essential for matrix assembly and budding. In contrast, the RNA-binding ring structures formed by VP40E-



I307R do not migrate to the membrane, assemble the viral matrix or bud VLPs. Currently, how the I307R mutation triggers VP40 ring formation or how wild-type VP40 transitions into a ring during infection remain unknown.

### **A conserved basic patch in the VP40 CTD is essential for assembly and budding of virus-like particles**

It has been previously shown that the C-terminal domain of VP40 is essential for electrostatic membrane interactions (Ruigrok et al., 2000). We hypothesized that basic residues in the CTDs of VP40 dimers were likely important for interacting with the negatively charged cytoplasmic leaflet of the cell membrane. We identified a basic surface on the VP40 CTD that is uniformly exposed on a single side of the VP40 dimer surface (Figure 4A). This basic patch is composed of six lysine residues (K221, K224, K225, K270, K274 and K275) and is conserved across the five species of ebolavirus (with one exception, K225 is R225 in Bundibugyo ebolavirus). We first targeted K224 and K225, as they reside in a flexible 10-residue loop which projects out from the CTD basic patch (disordered in all crystal structures of VP40). Initially we deleted the loop entirely, generating the mutant VP40E-<sup>221-229</sup>, and found that although expression levels and the dimeric structure were maintained, budding was abrogated (Figure S1, S5). We next returned only the residues 223-226 (GKKKG), generating VP40E-<sup>GKKKG</sup>, in which residues 221-222 and 227-229 remain deleted. The insertion of just the GKKKG component to VP40 restored wild-type budding activity (Figure 4C). To determine if it was the electrostatic charge of the KK motif that was important, we generated three mutants: VP40E-<sup>GMMG</sup> (neutral charge, similar in structure to lysine), VP40E-<sup>GEEG</sup> (negative charge), and VP40E-<sup>GRRG</sup> (positive charge). Only cells transfected with VP40 containing positively charged residues at positions 224 and 225 were able to efficiently assemble and bud VLPs (Figure 4). By contrast, cells transfected with VP40-<sup>GEEG</sup> or VP40-<sup>GMMG</sup> display a failure to properly interact with the membrane or bud VLPs (Figure 4C, 4D). These results suggest that the positive charge in positions 224 and 225 of the GKKKG-containing loop is essential to proper membrane interactions, matrix assembly and budding of virus-like particles.

To further confirm the involvement of this CTD basic patch in assembly, we mutated a second pair of conserved basic residues, K274 and K275, to yield VP40E-K274R/K275R (conserves positive charge) and VP40E-K274E/K275E (replaces with negative charge). As anticipated, VP40E-K274R/K275R buds at wild-type levels, while VP40E-K274E/K275E fails to bud any VLPs (Figure 4B). Interestingly, in contrast to VP40E-<sup>GMMG</sup> and VP40E-<sup>GEEG</sup>, VP40E-K274E/K275E clearly interacts with the cell membrane (Figure 4C) while displaying no matrix assembly activity at the cell surface (Figure 4D). The absence of any membrane ruffling by VP40E-K274E/K275E, in contrast to VP40E-M241R (Figure 3D), suggests that electrostatic interactions of VP40 with the cellular membrane may trigger a critical step in VP40 matrix assembly. This mechanism, which involves further VP40 oligomerization upon interaction with the membrane to drive matrix assembly and VLP budding is consistent with previously published work (Adu-Gyamfi et al., 2013; Scianimanico et al., 2000).

Together these results indicate that the conserved CTD basic patch is essential to membrane interactions and for triggering assembly of VP40 into the viral matrix to bud nascent virions. Additionally, the importance of the CTD basic surface indicates the most probable orientation and surface by which dimeric VP40 interacts with the cellular membrane.

### **A crystal structure of hexameric VP40 reveals how dimers further assemble into the viral matrix**

It has previously been shown that VP40 undergoes conformational change at the plasma membrane involving separation of the N- and C-terminal domains (Adu-Gyamfi et al., 2013; Gomis-Ruth et al., 2003; Scianimanico et al., 2000). Here, we have shown that the NTD-to-NTD interface that assembles the native VP40 dimer and the CTD-to-CTD interface by which dimers further assemble are both essential for matrix assembly and budding. However, these crystal structures were determined in the absence of phospholipids or electrostatically negative mimics. Although these structures display the dimeric interface, the CTD-CTD interface, and the basic surface that are all critical to matrix assembly (Figures 2, 3, 4), they do not account for the rotation of the CTD away from the NTD that is thought to occur at the cell membrane (Gomis-Ruth et al., 2003; Scianimanico et al., 2000). We wondered what effect interactions of the CTD basic patch with the cytoplasmic membrane leaflet may have on the structure of VP40 that could potentially trigger further oligomerization of VP40 into the viral matrix. Thus, we made a series of attempts to electrostatically satisfy the positively charged elements of the CTD basic patch by screening crystal conditions in the presence of various negatively charged additives. We found success when using dextran sulfate ( $M_r = 5$  kDa) as an additive. Of particular relevance, negatively charged dextran sulfate has been shown to outcompete binding of similarly charged phosphatidylserine, a known ligand of VP40 in the cell membrane (Ruigrok et al., 2000; Zschornig et al., 1993).

VP40E<sub>N</sub> crystals grown in the presence of dextran sulfate belong to the space group  $P4_21_2$  and diffract to 3.5 Å with three VP40 protomers (one and a half dimers) in the ASU. A crystallographic two-fold axis lies along the VP40 dimer interface joining the “half dimer” at the end of one ASU to the “half-dimer” at the start of the neighboring ASU to assemble a complete dimer. Thus, the biologically relevant unit present in these crystals is a hexameric structure comprised of three VP40 dimers (Figure 5). At each end of the hexamer is a VP40 protomer with its NTD and CTD in similar arrangement to those previously crystallized (Figure 5A). The remaining four VP40 protomers in center of the hexamer have undergone conformational changes that have separated their N- and C-terminal domains. The NTDs of these four protomers derive the central core of the hexamer and assemble through an interface which we refer to as the “oligomerization interface” (Figure 5A). This oligomerization interface is homologous to the “antiparallel dimer” interface previously observed in the context of the VP40 RNA-binding ring crystal structure (Gomis-Ruth et al., 2003). The oligomerization interface is centered on residue W95 and is revealed only through conformational displacement of the CTD away from the NTD (Figure 5B). After the conformational changes, the four CTDs extend out from the central core VP40 protomers in opposing directions (half are “up” and half are “down”). Electron density for the central core VP40 protomers is only observable for the NTDs, as the “sprung” CTDs linked to these



NTDs now extend into large solvent channels in the crystal packing and are disordered (Figure 5C). In the crystal, the VP40 hexamers also further assemble into uninterrupted filamentous structures via the same CTD-to-CTD interface described above (Figure 3), through the “unsprung” CTDs of adjacent ASUs (Figure 5C).

The observed filaments assembled from the VP40 hexamer provide a compelling model for ebolavirus matrix assembly, as they combine all of the biologically relevant VP40 surfaces and interfaces shown to be critical to matrix assembly: (1) the NTD-to-NTD dimeric interface involving L117 and T112 (Figure 2), (2) the CTD-to-CTD interface involving M241 and I307 (Figure 3), (3) the conserved, membrane-interacting CTD basic patches oriented along one single surface of the assembled filament (Figure 4, S6), and (4) the “oligomerization interface” by which the NTDs assemble the central core of the hexamer (Hoenen et al., 2010a).

### **The RNA-binding VP40 octameric ring plays a distinct role in the viral life cycle**

Previous work demonstrated that VP40 is capable of assembling an RNA-binding ring and that binding of RNA by VP40 is vital to the ebolavirus life cycle (Gomis-Ruth et al., 2003; Hoenen et al., 2005). Previous work also suggested that RNA is essential to maintaining the VP40 ring structure (Timmins et al., 2003). Here, however, we report a crystal structure of an RNA-free octameric VP40 ring. This RNA-free ring resulted from degradative loss of the CTDs within a crystal drop which originally contained purified, RNA-free ( $A_{260/280} < 0.6$ ), dimeric VP40E N (Figure 6). These crystals belong to the space group P422 and diffract to 1.85 Å. The RNA-free ring is nearly identical to the previously determined RNA-bound ring (Gomis-Ruth et al., 2003) and both are assembled by the same interfaces: the oligomerization interface, also observed in the VP40 hexamer, and another interface unique to the VP40 ring structure, which we term the “RNA-binding interface” (Figure 6A).

The RNA-free ring structure demonstrates that RNA is not structurally necessary to stabilize or assemble the VP40 ring. However, in order to verify whether RNA-free VP40 rings can assemble outside of a crystal, we generated two VP40 CTD deletion constructs: VP40E CTD and VP40E CTD-R134A. Purified VP40E CTD binds RNA ( $A_{260/280} > 1.0$ ) and displays a size exclusion chromatography elution profile consistent with formation of oligomeric rings in solution and with previous work (Gomis-Ruth et al., 2003). The R134A point mutation prevents RNA binding, and as anticipated, purified VP40E CTD-R134A is RNA-free ( $A_{260/280} < 0.6$ ). However, its size exclusion profile is consistent with that of VP40E CTD, demonstrating formation of RNA-free rings in solution (Figure S1). Taken together, RNA is likely critical to the displacement of the CTD from the NTD to trigger assembly of the ring structure, rather than necessary for the stability of the NTD-formed ring structure itself.

There is one consistent structural difference that appears to be critical to the formation of the VP40 octamer vs. the VP40 dimer and hexamer. As observed here and previously (Gomis-Ruth et al., 2003), the N-terminal 69 residues of VP40 need to move out of the dimeric interface in order for ring formation to occur (Figure 6B). This conformational change likely destabilizes the dimeric interface and exposes the RNA-binding interface (Figure 6C). Importantly, previous work showing the presence of VP40 rings in ebolavirus-infected cells

(Gomis-Ruth et al., 2003) and our full-length VP40E-I307R mutant which exclusively assembles VP40 rings, demonstrate that these conformational changes also occur in the context of full-length VP40.

The precise role of the VP40 RNA-binding ring in the viral life cycle has yet to be elucidated. Data presented here indicate that ring-forming VP40 does not traffic to the membrane, and is not required to bud VLPs (Figure 3). It has been suggested that the RNA-binding VP40 ring likely has a critical role outside virion assembly (Gomis-Ruth et al., 2003; Hoenen et al., 2005), possibly in negative regulation of viral transcription (Hoenen et al., 2010b). The discovery that our VP40E-I307R mutant exclusively assembles into rings allows us, for the first time, to unambiguously study the function of the full-length VP40 ring oligomer in the cell using ebolavirus mini-genome reporter assays (Figure 6D). Consistent with previous studies, we find WT-VP40E reduces transcription by ~70% compared to our normalized control (Hoenen et al., 2010b). Further, we find our VP40E-I307R ring-only mutant reduces viral transcription by ~80%. Thus, regulation of viral transcription is an activity tied to the RNA-binding ring structure, not dimeric VP40. Next, to determine if RNA binding by VP40 is critical to the observed reduction in transcription, we repeated the experiment with a double mutant incapable of RNA binding, VP40E-R134A/I307R, and only observed a ~30% reduction in transcription signal. Therefore, the RNA-binding activity of the VP40 ring structure is critical to the regulation of viral transcription observed with WT-VP40E and VP40E-I307R.

Since regulation of viral transcription is not directly linked to dimeric VP40, we were able to use the monomeric VP40E-L117R mutant to test whether dimeric VP40 is the precursor structure to the RNA-binding ring. If VP40 exists as a monomeric precursor as previously hypothesized (Dessen et al., 2000b), then assembly of the RNA-binding VP40 ring should still occur (L117R would be surface exposed in both monomer and ring) resulting in wild-type VP40 levels of transcriptional regulation. However, VP40E-L117R displays only a ~20% reduction in viral transcription, suggesting that dimeric VP40 is a necessary precursor to binding of RNA and assembly of the VP40 RNA-binding ring.

In summary, the results here show that the VP40 ring structure has a clear role in regulation of viral transcription through its RNA-binding activity, a role which is critical to the ebolavirus life cycle (Hoenen et al., 2005). Additionally, dimeric VP40 is an important precursor not only to matrix assembly, but also to binding of RNA and assembly of the VP40 RNA-binding ring.

## Discussion

How VP40 assembles the viral matrix and achieves its multiple roles in the ebolavirus life cycle has remained enigmatic. We discovered that VP40 is not a monomer as originally thought (Dessen et al., 2000b), but instead, is dimeric, and that the dimeric structure of VP40 is a critical precursor to matrix assembly and budding.

The VP40 dimer structure has a butterfly-like shape with a conserved basic patch in the CTD which is exposed across a single surface of the dimer. Removing the positive charge of

residues contained in the CTD basic patch abrogates assembly and budding of VLPs. The essential nature of this patch, coupled with the absence of a uniformly presented basic surface anywhere else on the VP40 dimer, suggests that the surface containing the CTD basic patches likely interacts with the negatively charged cytoplasmic leaflet of the cellular membrane. Interestingly, our basic patch mutants display different phenotypes in our IFA experiments. The VP40- GEEG mutant appears to migrate out from the nucleus toward the membrane but fails to interact with the membrane, while the VP40E-K274E/K275E mutant very clearly interacts with the cellular membrane. We hypothesize that the projecting VP40 GKKG loop is likely critical to initial interactions with, and orientation of VP40 to the membrane. We further hypothesize that as the VP40 dimer aligns along the membrane, residues K274 and K275 contact lipid and trigger conformational changes needed to assemble the viral matrix and bud nascent virions. This model is consistent with previously reported data (Adu-Gyamfi et al., 2012; Ruigrok et al., 2000; Scianimanico et al., 2000) and our EM micrographs that display a membrane ruffling phenotype with VP40E-M241R, but not with VP40E-K274E/K275E. These observations suggest that electrostatic interactions between the VP40 dimer and the membrane trigger a step in viral matrix assembly.

We also showed that co-crystallization of VP40 with dextran sulfate, a 5 kDa electrostatically negative mimic of the known VP40 membrane ligand phosphatidylserine (Ruigrok et al., 2000), triggers VP40 conformational rearrangements and assembly of VP40 dimers into a linear hexameric structure (Figure 4). The process by which the VP40 hexamer structure assembles likely involves multiple steps: (1) dimeric VP40 migrates to the membrane and interacts along the membrane in a uniform fashion via the basic patches on the CTDs, (2) VP40 dimers then begin to assemble with each other through CTD-to-CTD interactions, and (3) a twisting motion is induced, springing the CTD away from NTD to facilitate the anti-parallel assembly of VP40 dimers along the oligomerization interface observed in the VP40 hexamer (Movie S1). Recently, VP40 was shown to penetrate the cell membrane upon matrix assembly (Adu-Gyamfi et al., 2013). A twisting motion could lend the force needed push the CTD into the cell membrane.

In crystals, the VP40 hexamers assemble into continuous filaments via the conserved M241- and I307-containing CTD-CTD interface (Figure 7, S6). In this arrangement, hexameric VP40 creates a filamentous multi-layered assembly. A central or core layer is derived from repeating VP40 hexamers. Two other layers, sandwiching the core, are formed by the CTDs that spring up or down from the four NTDs at the core of each hexamer. We believe this arrangement may reflect how the filovirus matrix is assembled. CTDs of VP40 are known to interact with both the membrane on the outside of the virion and also the nucleocapsid at the center of the virion. The crystal structure, in which CTDs spring alternately up or down explains how this could occur. The “upper” layer of CTDs could interact with the viral membrane, while the “lower” layer of CTDs could interact with the viral nucleocapsid (Figure 7A).

Recent tomographic analysis of filovirus virions demonstrates that VP40 indeed assembles into a multi-layered matrix (Bharat et al., 2011), reflected in our model. In tomography, density for the outer layer may have merged a bit with the membrane; as in biophysical studies, the CTDs are observed to partially penetrate membrane. In tomography, a “space”

between the core matrix layer is observed; in our model, the N-terminal domains of the hexamer-assembled core do not lie directly against the membrane after conformational changes have occurred (Beniac et al., 2012; Bharat et al., 2011). Instead, the outer layer is bridged to the core layer by the flexible linkers of the CTDs, which are not electron dense.

Further, tomographic studies observe repeating structural features along the axis of the virion that closely correspond to repeating features observed in the VP40 hexamer: ~5 nm (width of NTD dimer) and ~7 nm (length of repeating ASUs in hexamer-assembled filaments) (Beniac et al., 2012; Bharat et al., 2011). Tomographic 2D averages of the VP40 matrix from ebolavirus suggests the matrix has a somewhat flexible and pleomorphic, but generally repeating structure (Beniac et al., 2012). Individual VP40 filaments assembled by repeating hexamers in the crystal packing match the observed repeating density array in 2D averages from equivalent tomographic slices (Figure 7B).

A remaining question is whether, in the actual viral matrix, all CTDs have sprung and the central core is made only from NTDs, or if the central core layer is assembled from repeating hexamers at each end. We believe that CTD-CTD interactions are likely involved in the core matrix layer. Only the CTD-CTD interface provides a slippery, flexible surface. All NTD-NTD interfaces visualized thus far are rigid. An NTD-only filament, in the absence of any CTD-CTD interfaces contained at any interval within it, would likely present a rigid, uniform structure, inconsistent with the flexible and pleomorphic nature of the filovirus virion (Bharat et al., 2011; Kuhn, 2008). Further, our mutagenesis to the CTD (Figure 3) and previous work demonstrating lipid-induced assembly of VP40 hexamers (Scianimanico et al., 2000), suggest that CTD-to-CTD interactions and discrete hexameric units, as are bounded by this interaction, are both critical parts of the ebolavirus matrix structure.

Until now, the roles of RNA binding and the resulting VP40 ring structures in the viral life cycle have remained elusive. This was primarily due to the fact that studying VP40 ring formation in the cell required either truncating the CTD or utilizing indirect methodology (Hoenen et al., 2010a). Here, the I307R mutation allowed us to unambiguously characterize the cellular function of full-length VP40 in its oligomeric ring state. We found that when VP40 is bound to RNA and adopts the ring structure, it assumes a perinuclear location. Moreover, our mini-genome assays now demonstrate that binding of RNA by VP40 and the RNA-binding ring structure confer the transcriptional control function. Recent studies demonstrate that in the early stages of ebolavirus infection, VP40 first participates in the formation of perinuclear structures with additional viral proteins (Nanbo et al., 2013). Thus, we propose that VP40 RNA binding is critical to the initial stages of viral transcription upon infection. This is consistent with previous data indicating recombinant viruses with a VP40 RNA-binding knockout mutation (R134A) fail to replicate (Hoenen et al., 2005). The mechanism by which VP40 transitions from a dimer to a ring structure during an infection remains elusive and is the topic of continued investigation. Although RNA is not required to form a ring from CTD-deleted VP40, it may play a role in displacement of NTD and CTD from each other in natural infection. A hypothesis for how dimeric VP40 transitions into the ring structure is modeled in Movie S2.

The results presented here illustrate how the VP40 protein performs multiple distinct roles in the ebolavirus life cycle. Through structural rearrangements, VP40 assembles multiple distinct structures with unique and essential functions. It is known that viral proteins are multifunctional, but our work on VP40 calls into question the belief that a single viral protein structure or assembly is responsible for all the known functions of that protein. Viruses, particularly RNA viruses, can be subject to limitations on genomic size. By encoding proteins that can structurally rearrange themselves to operate at different stages of the life cycle, viruses like the ebolaviruses can accomplish a multitude of essential functions with a limited number of genes. Further, other viral matrix proteins, such as M of respiratory syncytial virus and M1 of influenza virus, are also constructed via discrete NTDs and CTDs connected by a long linker, bind RNA, and regulate viral transcription (Baudin et al., 2001; Money et al., 2009). Hence, other viruses may encode proteins capable of similar structural transformations.

The structure-shifting properties of VP40 provide novel opportunities for the development of antiviral drugs. For example, small molecules capable of influencing the propensity of one VP40 structure over another (as seen with VP40E-I307R) could severely impede the ebolavirus life cycle. VP40 thus provides a model for how viruses with small genomes, like ebolaviruses, can accomplish a multitude of essential functions with a limited number of proteins.

## Experimental Procedures

### Protein Expression and Purification

VP40S<sub>N</sub> and VP40E<sub>N</sub> (and VP40E<sub>N</sub> mutants) were expressed in BL-21 Rosetta 2 *E.coli* cell using the pET-46 Ek/LIC vector. For details, see Extended Experimental Procedures.

### Western Blots

293 cells were transfected with a pTRIEX 5 plasmid expressing WT-VP40E or a mutant VP40E. Analysis was carried out 24 hours post transfection. For details, see Extended Experimental Procedures.

### Confocal Microscopy

293 cells were transfected with a pCAGGS plasmid expressing WT-VP40E or a mutant VP40E. Analysis was carried out 24 hours post-transfection. For more detail, see Extended Experimental Procedures.

Other methods are described in the Extended Experimental Procedures online.

## Supplementary Material

Refer to Web version on PubMed Central for supplementary material.

## Acknowledgments

We thank the beamline scientists at APS 19-ID and GM/CA 23-ID, SSRL 12-2, and ALS 5.0.2, Dr. Jean-Philippe Julien for assistance with the SEC-MALS analysis, Christina Corbaci for the graphical abstract, and Dr. Glen Nemerow and Dr. B.V.V Prasad for helpful comments and suggestions. E.O.S. was supported by a Career Award in the Biomedical Sciences and an Investigator in the Pathogenesis of Infectious Disease award from the Burroughs Wellcome Fund, The Skaggs Institute of Chemical Biology and NIAID R43 AI1088843. Z.A.B. was supported by 2T32AI007244 to the TSRI Dept. of Immunology and Microbial Science. Y.K. acknowledges membership within and support from the Region V 'Great Lakes' Regional Center for Excellence (RCE) for Biodefense and Emerging Infectious Disease Research Program (NIH award U54 AI057153). T.N. was supported by a Grant-in-Aid for Young Scientists from the Japan Society for the Promotion of Science and by a Grant-in-Aid for Scientific Research on Priority Areas from the Ministry of Education, Culture, Sports, Science, and Technology. This is manuscript #21649 from The Scripps Research Institute. Coordinates and Structure Factors have been deposited into the Protein Data Bank under accession codes 4LD8, 4LDB, 4LDD, 4LDI, and 4LDM.

## References

- Adu-Gyamfi E, Digman MA, Gratton E, Stahelin RV. Investigation of Ebola VP40 assembly and oligomerization in live cells using number and brightness analysis. *Biophysical journal*. 2012; 102:2517–2525. [PubMed: 22713567]
- Adu-Gyamfi E, Soni SP, Xue Y, Digman MA, Gratton E, Stahelin RV. The Ebola virus matrix protein penetrates into the plasma membrane: A key step in VP40 oligomerization and viral egress. *The Journal of biological chemistry*. 2013
- Baudin F, Petit I, Weissenhorn W, Ruigrok RW. In vitro dissection of the membrane and RNP binding activities of influenza virus M1 protein. *Virology*. 2001; 281:102–108. [PubMed: 11222100]
- Beniac DR, Melito PL, Devarenes SL, Hiebert SL, Rabb MJ, Lamboo LL, Jones SM, Booth TF. The organisation of ebola virus reveals a capacity for extensive, modular polyploidy. *PLoS One*. 2012; 7:e29608. [PubMed: 22247782]
- Bharat TA, Riches JD, Kolesnikova L, Welsch S, Krahling V, Davey N, Parsy ML, Becker S, Briggs JA. Cryo-electron tomography of Marburg virus particles and their morphogenesis within infected cells. *PLoS Biol*. 2011; 9:e1001196. [PubMed: 22110401]
- Bwaka MA, Bonnet MJ, Calain P, Colebunders R, De Roo A, Guimard Y, Katwili KR, Kibadi K, Kipasa MA, Kuvula KJ, et al. Ebola hemorrhagic fever in Kikwit, Democratic Republic of the Congo: clinical observations in 103 patients. *J Infect Dis*. 1999; 179(Suppl 1):S1–7. [PubMed: 9988155]
- Dessen A, Forest E, Volchkov V, Dolnik O, Klenk HD, Weissenhorn W. Crystallization and preliminary X-ray analysis of the matrix protein from Ebola virus. *Acta Crystallogr D Biol Crystallogr*. 2000a; 56:758–760. [PubMed: 10818356]
- Dessen A, Volchkov V, Dolnik O, Klenk HD, Weissenhorn W. Crystal structure of the matrix protein VP40 from Ebola virus. *EMBO J*. 2000b; 19:4228–4236. [PubMed: 10944105]
- Geisbert TW, Jahrling PB. Differentiation of filoviruses by electron microscopy. *Virus Res*. 1995; 39:129–150. [PubMed: 8837880]
- Gomis-Ruth FX, Dessen A, Timmins J, Bracher A, Kolesnikowa L, Becker S, Klenk HD, Weissenhorn W. The matrix protein VP40 from Ebola virus octamerizes into pore-like structures with specific RNA binding properties. *Structure*. 2003; 11:423–433. [PubMed: 12679020]
- Harty RN. No exit: targeting the budding process to inhibit filovirus replication. *Antiviral Res*. 2009; 81:189–197. [PubMed: 19114059]
- Harty RN, Brown ME, Wang G, Huibregtse J, Hayes FP. A PPxY motif within the VP40 protein of Ebola virus interacts physically and functionally with a ubiquitin ligase: implications for filovirus budding. *Proc Natl Acad Sci U S A*. 2000; 97:13871–13876. [PubMed: 11095724]
- Hoenen T, Biedenkopf N, Ziebeck F, Jung S, Groseth A, Feldmann H, Becker S. Oligomerization of Ebola virus VP40 is essential for particle morphogenesis and regulation of viral transcription. *J Virol*. 2010a; 84:7053–7063. [PubMed: 20463076]
- Hoenen T, Jung S, Herwig A, Groseth A, Becker S. Both matrix proteins of Ebola virus contribute to the regulation of viral genome replication and transcription. *Virology*. 2010b; 403:56–66. [PubMed: 20444481]



- Hoenen T, Volchkov V, Kolesnikova L, Mittler E, Timmins J, Ottmann M, Reynard O, Becker S, Weissenhorn W. VP40 octamers are essential for Ebola virus replication. *J Virol.* 2005; 79:1898–1905. [PubMed: 15650213]
- Jasenosky LD, Neumann G, Lukashevich I, Kawaoka Y. Ebola virus VP40-induced particle formation and association with the lipid bilayer. *J Virol.* 2001; 75:5205–5214. [PubMed: 11333902]
- Johnson RF, Bell P, Harty RN. Effect of Ebola virus proteins GP, NP and VP35 on VP40 VLP morphology. *Viol J.* 2006; 3:31. [PubMed: 16719918]
- Kuhn, JH. *Archives of virology.* SpringerWeinNew York; Wien; New York: 2008. Filoviruses: a compendium of 40 years of epidemiological, clinical, and laboratory studies; p. 23-50.
- Kuhn JH, Bao Y, Bavari S, Becker S, Bradfute S, Brister JR, Bukreyev AA, Cai Y, Chandran K, Davey RA, et al. Virus nomenclature below the species level: a standardized nomenclature for laboratory animal-adapted strains and variants of viruses assigned to the family Filoviridae. *Arch Virol.* 2013
- Money VA, McPhee HK, Mosely JA, Sanderson JM, Yeo RP. Surface features of a Mononegavirales matrix protein indicate sites of membrane interaction. *Proc Natl Acad Sci U S A.* 2009; 106:4441–4446. [PubMed: 19251668]
- Nanbo A, Watanabe S, Halfmann P, Kawaoka Y. The spatio-temporal distribution dynamics of Ebola virus proteins and RNA in infected cells. *Scientific reports.* 2013; 3:1206. [PubMed: 23383374]
- Noda T, Sagara H, Suzuki E, Takada A, Kida H, Kawaoka Y. Ebola virus VP40 drives the formation of virus-like filamentous particles along with GP. *J Virol.* 2002; 76:4855–4865. [PubMed: 11967302]
- Panchal RG, Ruthel G, Kenny TA, Kallstrom GH, Lane D, Badie SS, Li L, Bavari S, Aman MJ. In vivo oligomerization and raft localization of Ebola virus protein VP40 during vesicular budding. *Proc Natl Acad Sci U S A.* 2003; 100:15936–15941. [PubMed: 14673115]
- Ruigrok RW, Schoehn G, Dessen A, Forest E, Volchkov V, Dolnik O, Klenk HD, Weissenhorn W. Structural characterization and membrane binding properties of the matrix protein VP40 of Ebola virus. *J Mol Biol.* 2000; 300:103–112. [PubMed: 10864502]
- Scianimanico S, Schoehn G, Timmins J, Ruigrok RHW, Klenk HD, Weissenhorn W. Membrane association induces a conformational change in the Ebola virus matrix protein. *Embo Journal.* 2000; 19:6732–6741. [PubMed: 11118208]
- Timmins J, Schoehn G, Kohlhaas C, Klenk HD, Ruigrok RW, Weissenhorn W. Oligomerization and polymerization of the filovirus matrix protein VP40. *Virology.* 2003; 312:359–368. [PubMed: 12919741]
- Wyatt PJ. Submicrometer Particle Sizing by Multiangle Light Scattering following Fractionation. *Journal of colloid and interface science.* 1998; 197:9–20. [PubMed: 9466838]
- Zschornig O, Arnold K, Ohki S. Effect of glycosaminoglycans and PEG on fusion of Sendai virus with phosphatidylserine vesicles. *Biochim Biophys Acta.* 1993; 1148:1–6. [PubMed: 8388724]

**Highlights**

- VP40 is a dimer; the dimer structure is critical for trafficking and matrix assembly.
- Charged interactions between VP40 and the cell membrane induce matrix assembly.
- A hexameric VP40 crystal structure demonstrates how the viral matrix is assembled.
- VP40 forms a different, RNA-binding ring structure to regulate viral transcription.

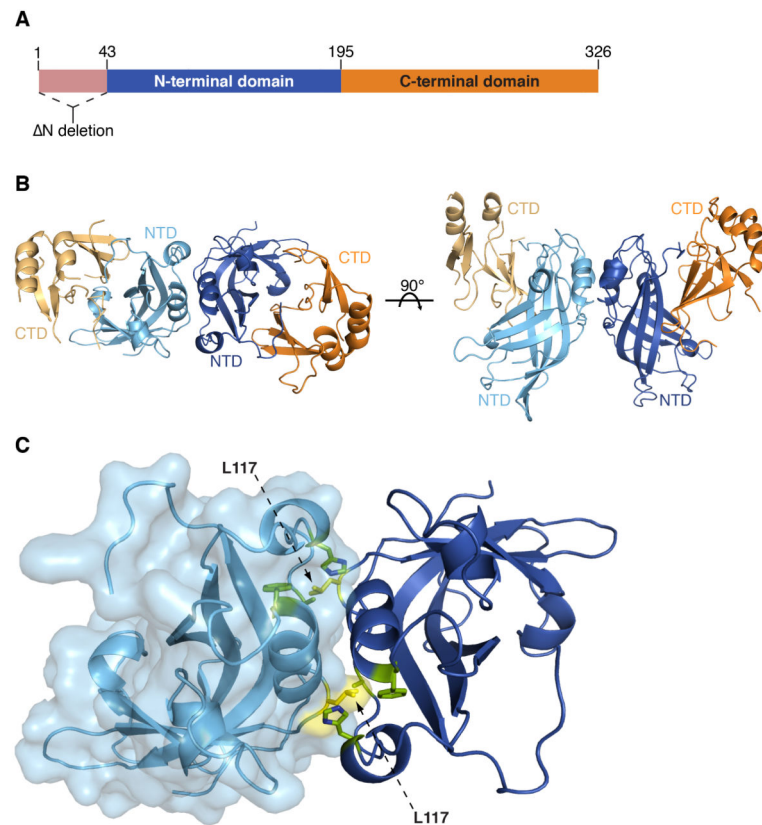


**Figure 1. The dimeric structure of VP40**

(A) A schematic of VP40 showing the location of the N-terminal 43 residue deletion in VP40S<sup>N</sup> and VP40E<sup>N</sup> and the NTD (blue) and CTD (orange). (B) The VP40E<sup>N</sup> dimeric crystal structure is displayed with the NTDs from each protomer colored light or dark blue and CTDs light or dark orange. (C) The VP40E<sup>N</sup> dimeric interface displaying residues A55, H61, F108, A113 and M116 (green) and L117 (yellow). The surface representation on the light blue protomer illustrates how L117 reaches into the opposing protomer. See also **Figure S1** and **S2**.

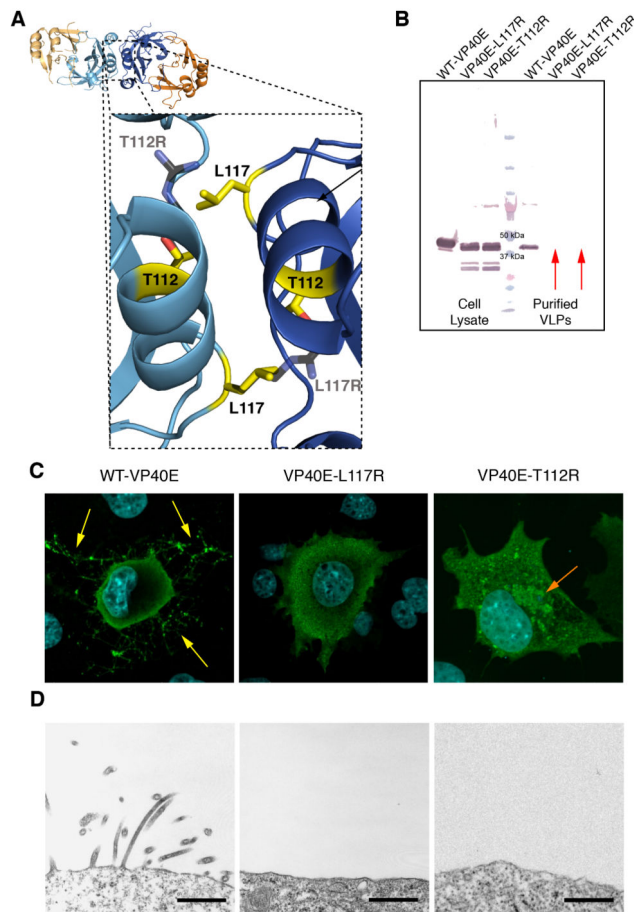


**Figure 2. Analysis of the VP40 dimeric interface**

(A) A dashed box displays a close-up view of the dimeric interface, centered on residues T112 and L117 (yellow). The point mutations T112R and L117R have been modeled onto the structure (black). (B) Western blot of cell lysates and purified VLPs from transfected cells. VP40E-L117R and VP40E-T112R do not bud VLPs from transfected cells (red arrows). (C) IFA experiments show WT-VP40E localizes to the cell membrane and buds VLPs (yellow arrows), while both VP40E-L117R and VP40E-T112R fail to localize to the membrane or assemble and bud VLPs. VP40E-T112R also forms perinuclear structures (orange arrow). (D) EM micrographs display active VLP assembly and budding from cells transfected with WT-VP40E, while cells transfected with either VP40E-L117R or VP40E-T112R display no assembly or VLP budding activity. \*Scale bars = 500 nm.

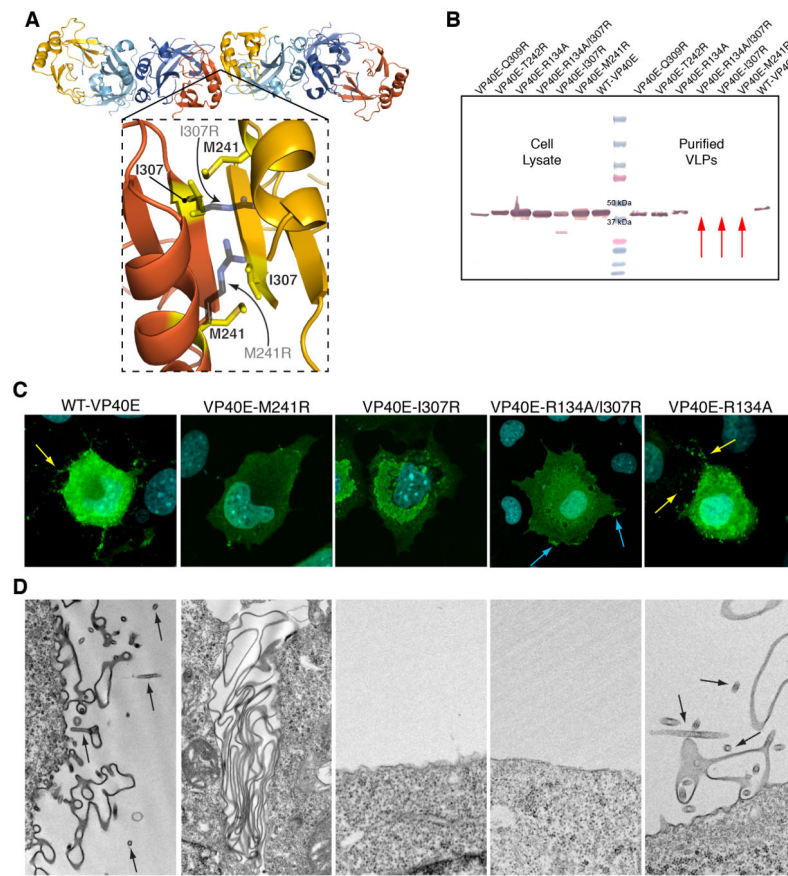


**Figure 3. Analysis of the VP40 CTD-to-CTD interface**

(A) The CTD-to-CTD interface between VP40 dimers is shown with the NTDs from each protomer colored light or dark blue and CTDs colored light or dark orange. Below, a view of the CTD-to-CTD interface around residues M241 and I307 (yellow) with the disruptive mutations M241R and I307R (black) modeled onto the orange CTD. (B) Western blot of cell lysates and purified VLPs from transfected cells. Disruptive CTD-to-CTD interface point mutants, VP40E-M241R, VP40E-I307R and VP40E-R134A/I307R, fail to bud VLPs (red arrows). The CTD control mutants, VP40E-T242R and VP40E-Q309R, successfully assemble and bud VLPs. (C) IFA of transfected cells show dimeric WT-VP40E and VP40E-R134A migrate to the cell membrane and bud VLPs (yellow arrows). In contrast, VP40E-M241R and VP40E-R134A/I307R, bearing point mutations to the CTD-to-CTD interface, similarly migrate to the cell membrane but do not bud VLPs. Patches of VP40E-R134A/I307R accumulated at the membrane are indicated by blue arrows. VP40E-I307R, which exclusively forms rings, does not migrate to the membrane, but instead forms perinuclear structures. (D) EM micrographs show WT-VP40E and VP40E-R134A cause typical membrane ruffling, assembly and budding of filamentous VLPs (black arrows). VP40E-M241R displays an exaggerated wild-type VP40 membrane ruffling morphology, yet the cell surface remains devoid of budding filamentous VLPs. VP40E-I307R and VP40E-R134A/I307R display no membrane ruffling, matrix assembly or budding activity. See also Figure S3 and S4. \*Solid scale bars = 1  $\mu$ m and the dashed scale bars = 500 nm.

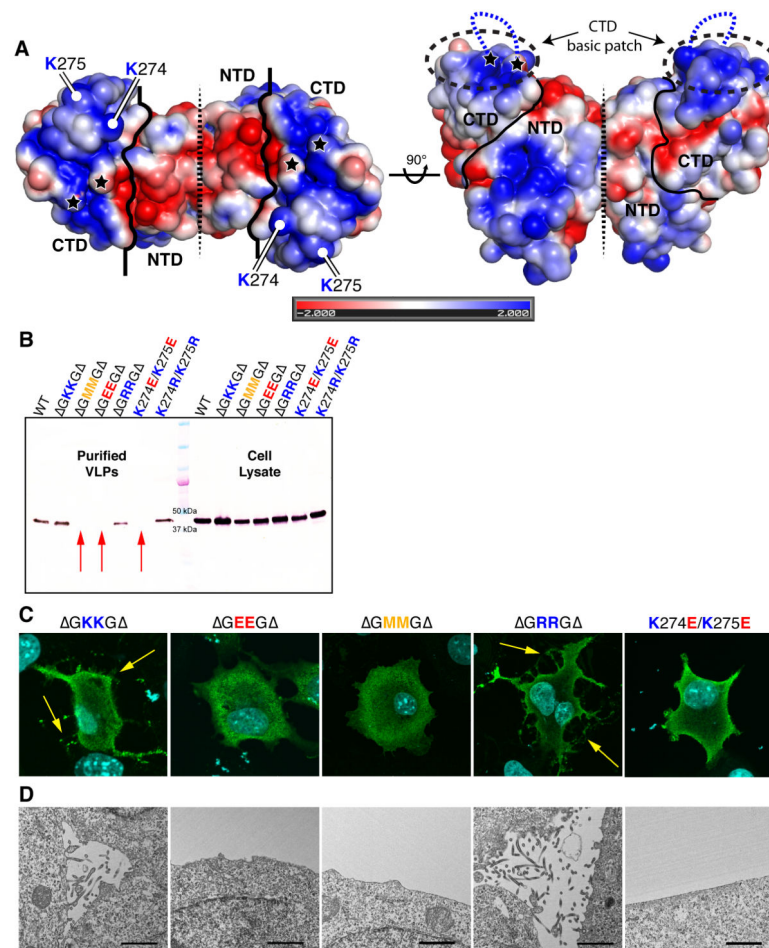


**Figure 4. Characterization of VP40 basic patch**

(A) Electrostatic surface potential of the VP40E N dimer in two orientations. The dimer interface is indicated by a dashed line and the division of the NTD and CTD is depicted by a solid black line. The attachment points of the disordered GKKG loop are indicated by stars and the loop is modeled as a broken blue line (on right). (B) Western blot of cell lysates and purified VLPs from transfected cells. The VP40E- GMMG , VP40E- GEEG and VP40E-K274E/K275E constructs express, but fail to assemble or bud VLPs (red arrows). (C) IFA demonstrates that VP40E- GKKG and VP40E- GRRG assemble and bud VLPs (yellow arrows). By contrast, VP40E- GEEG and VP40E- GMMG fail to interact with the membrane. While VP40E-K274E/K275E clearly migrates to and interacts with the cell membrane, but fails to assemble and bud VLPs. (D) EM micrographs display active VLP assembly and budding for VP40E- GKKG and VP40E- GRRG , but no assembly or VLP budding for VP40E- GEEG , VP40E- GMMG , or VP40E-K274E/K275E. See also Figure S5 and Movie S1. \*Scale bars = 500 nm.



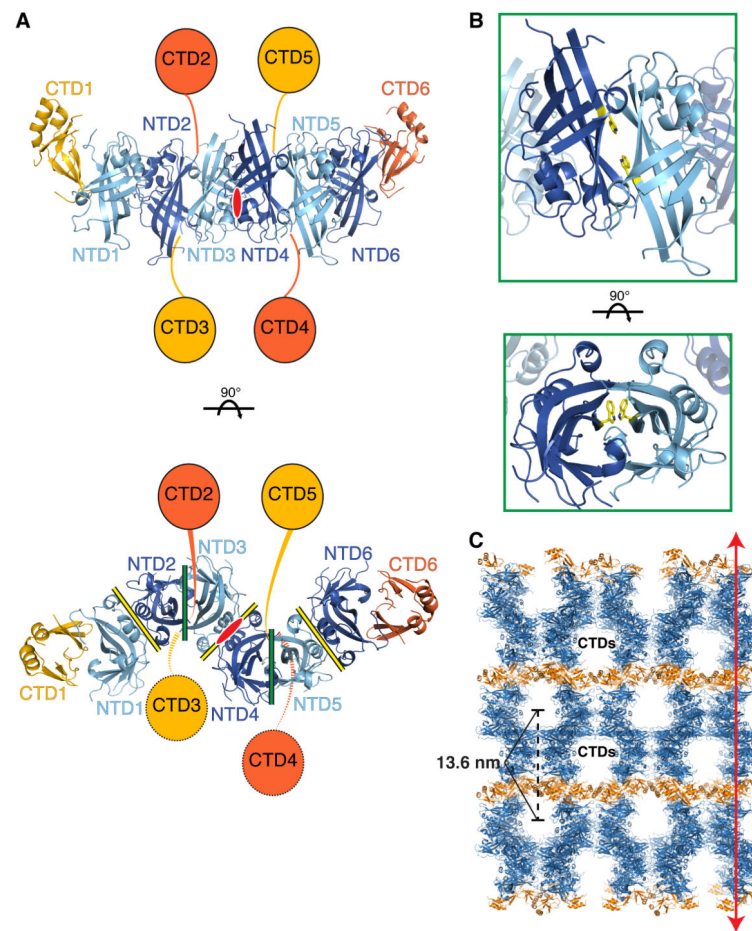


**Figure 5. Hexameric VP40 crystal structure**

(A) The VP40E N hexamer structure assembled across a crystallographic 2-fold axis (red oval), is illustrated with the NTDs colored alternatively in light or dark blue and the CTDs colored in light or dark orange. The NTDs and CTDs are numbered according to the protomer to which they belong. The disordered “sprung” CTDs are modeled as circles (to scale). Below, a 90° rotation in which the dimeric and oligomeric interfaces are indicated by yellow and green lines, respectively. (B) The oligomerization interface is displayed from the VP40 hexamer, centered on residue W95 (yellow). (C) A section of the VP40E N hexamer crystal packing is shown, the NTD is colored blue and the CTD is colored orange. Here the uninterrupted filament structures formed via the CTD-to-CTD interface (one filament indicated by a red line) as well as the large solvent channels that contain the “sprung” CTDs can be seen.

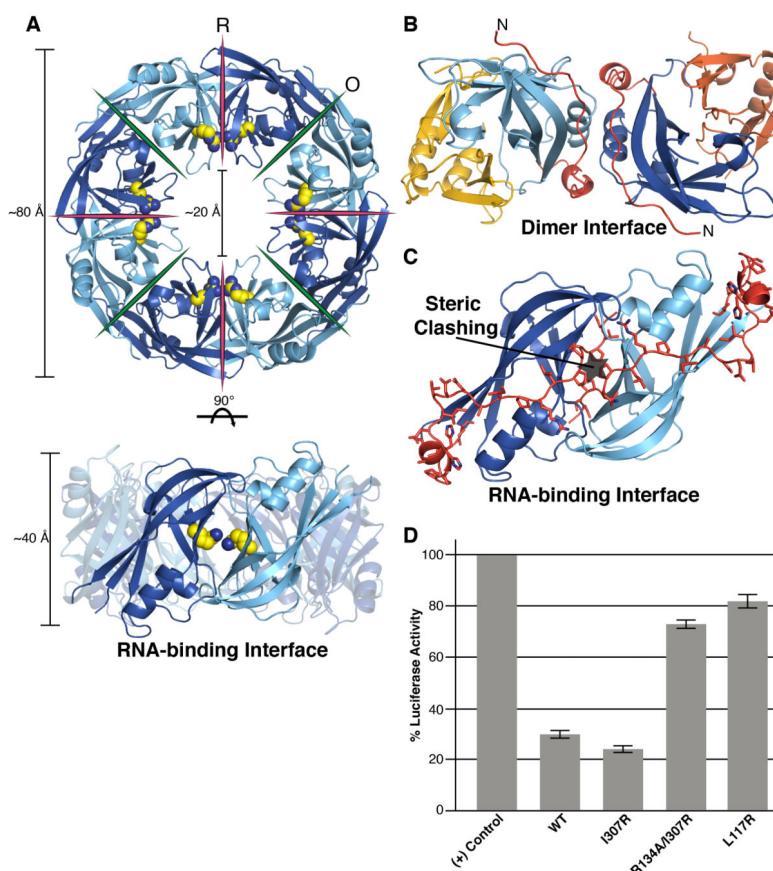


**Figure 6. Analysis of the octameric VP40 ring structure**

(A) Crystal structure of the RNA-free VP40 octameric ring, with alternating NTD protomers colored in light and dark blue. Residue R134 is depicted by yellow spheres. The oligomeric interface and RNA-binding interface are indicated by green and pink lines respectively. (B) The VP40E N dimer. Opposing NTDs are colored light or dark blue, and the CTDs are colored light or dark orange. Residues 45-70 in the dimer interface are colored red. (C) By alignment of the NTDs from dimeric VP40 and RNA-bound VP40, we have modeled residues 45-70 ordered in the dimer (red) onto the RNA-binding interface. The alignment demonstrates how assembly of the RNA-binding interface would be obstructed unless residues 1-70 unraveled from the NTD structure. (D) Mini-genome reporter assays were performed in triplicate and data normalized to a positive control expressing Renilla Luciferase to reflect transcription levels of 100%. WT-VP40E reduces transcription by ~70% with a standard deviation (SD) of 3.7% and VP40E-I307R reduces transcription by ~80% (SD = 2.6%) respectively. In contrast, VP40E-R134A/I307R and VP40E-L117R only reduce levels of transcription by ~30% (SD = 3.3%) and ~20% (SD = 5.3%) respectively. See also Movie S2.

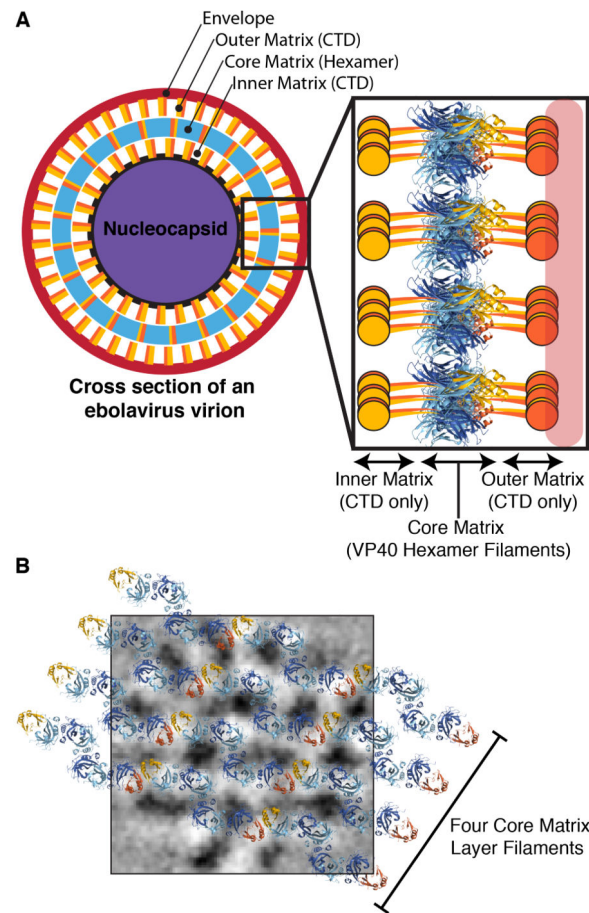


**Figure 7. Model of the VP40 matrix**

(A) A cross-section of an ebolavirus virion is modeled by assembly of VP40 (NTD colored blue, CTD colored light or dark orange) into a multi-layered matrix as predicted by our hexameric crystal structure and by tomography studies (Beniac et al., 2012; Bharat et al., 2011). The black box on the cross section corresponds to the dashed box containing a four-filament assembly. In this model, the crystal structure of the hexamer-assembled filament forms the core layer of the matrix. The basic patches of the hexamer CTDs are positioned toward the outer membrane and the “sprung” CTDs form the inner matrix layer and outer matrix layer (upper left of panel A). (B) Four individual VP40 filaments derived from the assembly VP40 hexamers are modeled to scale onto 2D averages. Black/white has been inverted for clarity in these images, white now corresponds to VP40 density (adapted from Beniac et al., 2012). See also Figure S6.